J|A|C|S ARTICLES

Published on Web 08/31/2010

Scrutinizing the Chemical Nature and Photophysics of an Expanded Hemiporphyrazine: The Special Case of [30]Trithia-2,3,5,10,12,13,15,20,22,23,25,30-dodecaazahexaphyrin

Olga N. Trukhina,[†,¶] M. Salomé Rodríguez-Morgade,[†] Silke Wolfrum,[‡] Esmeralda Caballero,[†] Natalia Snejko,[§] Elena A. Danilova,[¶] Enrique Gutiérrez-Puebla,[*,§] Mikhail K. Islyaikin,[*,¶] Dirk M. Guldi,[*,‡] and Tomás Torres[*,†,≠]

Departamento de Química Orgánica (C−I), Universidad Autónoma de Madrid, Cantoblanco, 28049 Madrid, Spain, Friedrich-Alexander-Universität Erlangen-Nürnberg, Interdisciplinary Center for Molecular Materials (ICMM), Egerlandstrasse 3, D-91058 Erlangen, Germany, Instituto de Ciencia de Materiales de Madrid, CSIC, Sor Juana Inés de la Cruz 3, E-28049 Madrid, Spain, Department of Fine Organic Synthesis, Ivanovo State University of Chemistry and Technology, 153000 Ivanovo, Russia, and IMDEA-Nanociencia, Facultad de Ciencias, Cantoblanco, 28049 Madrid, Spain

Received May 26, 2010; E-mail: tomas.torres@uam.es; dirk.guldi@chemie.uni-erlangen.de; egutierrez@icmm.csic.es; islyaikin@isuct.ru

Abstract: Thirty π-electron-expanded hemiporphyrazines **1a**−**c** have been prepared by crossover condensation reaction of 2,5-diamino-1,3,4-thiadiazole and the corresponding phthalonitrile (**3**) or diiminoisoindoline (**4**) derivatives. The expanded azaporphyrin hexamers have been unequivocally characterized by means of spectroscopic, crystallographic, and electrochemical techniques. Weak intramolecular hydrogen bonding imposes a planar conformation to macrocycles. However, the overall electronic delocalization is low, and the nature of the resulting [30]heteroannulene is nonaromatic, as confirmed by NMR studies, XR diffraction analysis, and calculation of the NICS(0) value. Studies on a wide range of physicochemical features including ground, excited, reduced, and oxidized states provide evidence for the wide applicability of these 30 π-electron-expanded hemiporphyrazines in processes involving electron transfer. A key asset of our work is the systematic development of spectroscopic and kinetic markers for the formation and decay of all of the aforementioned species. Thirty π-electron-expanded hemiporphyrazines evolve as broadly absorbing light harvesters with excited state energies of around 2.3 eV that are susceptible to facile one-electron reduction and one-electron oxidation reactions.

Introduction

Aromaticity is a manifestation of electron delocalization in closed circuits, and its definition and quantification are current topics of great interest.[1] In this respect, expanded porphyrinoids are resulting in excellent models by which to study the case of heteroannulenes.[2−4] Indeed, since the discovery of sapphyrin by Woodward,[5] expanded porphyrins have fascinated researchers from a pure, academic point of view, because they constitute ideal models to explore the limits of the classical Hückel rule to define aromaticity.[2,3] Moreover, their conformational flexibility allows them to adopt the hitherto elusive Möbius topology,[3e] affording Möbius aromatic and even antiaromatic systems.[4] The design of expanded porphyrins is also interesting from a functional viewpoint, since their structural makeup provides them with features that are virtually inaccessible for the corresponding tetramers. For example, they possess exceptional coordination properties[2,3,6,7] such as the ability to ac-

[†] Departamento de Química Orgánica, Universidad Autónoma de Madrid.
[¶] Ivanovo State University of Chemistry and Technology.
[‡] Friedrich-Alexander-Universität Erlangen-Nürnberg.
[§] Instituto de Ciencia de Materiales de Madrid, CSIC.
[≠] IMDEA-Nanociencia.

(1) (a) von Ragué Schleyer, P. *Chem. Rev.* **2001**, *101*, 1116–1118, and references therein. (b) von Ragué Schleyer, P. *Chem. Rev* **2005**, *105*, 3433–3435, and references therein.

(2) (a) Jasat, A.; Dolphin, D. *Chem. Rev.* **1997**, *97*, 2267–2340, and references cited therein. (b) Sessler, J. L.; Weghorn, S. J. *Expanded, Contracted and Isomeric Porphyrins*; Pergamon: New York, 1997. (c) Sessler, J. L.; Gebauer, A.; Weghorn, S. J. Expanded Porphyrins. In *Heteroporphyrins, Expanded Porphyrins and Related Macrocycles*; Kadish, K. M., Smith, K. M., Guilard, R., Eds.; The Porphyrin Handbook, Vol. 2, Chapter 9; Academic Press: San Diego, CA, 2000; pp 55−124. (d) Lash, T. D. Syntheses of Novel Porphyrinoid Chromophores. In *Heteroporphyrins, Expanded Porphyrins and Related Macrocycles*; Kadish, K. M., Smith, K. M., Guilard, R., Eds.; The Porphyrin Handbook, Vol. 2, Chapter 10; Academic Press: San Diego, CA, 2000; pp 125−199.

(3) (a) Sessler, J. L.; Seidel, D. *Angew. Chem., Int. Ed.* **2003**, *42*, 5134–5175. (b) Chandrashekar, T. K.; Venkatraman, S. *Acc. Chem. Res.* **2003**, *36*, 676–691. (c) Shimizu, S.; Osuka, A. *Eur. J. Inorg. Chem.* **2006**, 1319–1335. (d) Misra, R.; Chandrashekar, T. K. *Acc. Chem. Res.* **2008**, *41*, 265–279. (e) Jux, N. *Angew. Chem., Int. Ed.* **2008**, *47*, 2543–2546.

(4) (a) Stepien, M.; Latos-Grazÿynski, L.; Sprutta, N.; Chwalisz, P.; Szterenberg, L. *Angew.Chem., Int. Ed.* **2007**, *46*, 7869–7873. (b) Yoon, Z. S.; Osuka, A.; Kim, D. *Nature Chem.* **2009**, *1*, 113–122, and references therein. (c) Aihara, J.-i.; Horibe, H. *Org. Biomol. Chem* **2009**, *7*, 1939–1943. (d) Lim, J. M.; Yoon, Z. S.; Shin, J. Y.; Kim, K. S.; Yoon, M.-C.; Kim, D. *Chem. Commun* **2009**, 261–273.

commodate large cations—i.e. lanthanides and actinides—[6b,7] and this feature is particularly appealing in the field of magnetic resonance imaging (MRI) and nuclear remediation technologies, respectively. Their large central cavities can also function as anion receptors; therefore, expanded analogues are pursued for anion sensing and transport.[2,3,8] Finally, expanded macrocycles possess extended conjugated π-systems that are associated to red-shifted absorptions in the visible region,[9] and hence, they are potentially useful as therapeutic agents in photodynamic therapy (PDT) or radiotherapy[10] as nonlinear optical materials,[4d,11] and in optical limiting.[12] All these incentives and others[13] have motivated researchers to design and synthesize a large assortment of expanded porphyrinoids. Parallel to that of porphyrins, the chemistry of tetraazaporphyrins and, particularly, that of phthalocyanines has registered a huge progress in the last century.[14] Conversely, their related expanded congeners have been hardly explored. One of the main obstacles for the rational design of expanded azaporphyrins is the proclivity of the corresponding tetramers to be formed, so their arrangement competes and, in most cases, excludes the formation of other larger macrocycles or open-chain intermediates. Superphthalocyanines represent an exception.[15] In fact, these pentapyrrolic macrocycles constituted for many years the only reported expanded azaporphyrins.

Scheme 1. Synthesis of the Expanded Hemiporphyrazines **1a**−**c** (Only the Major C_3 Isomer of **1a** is Represented for Clarity)

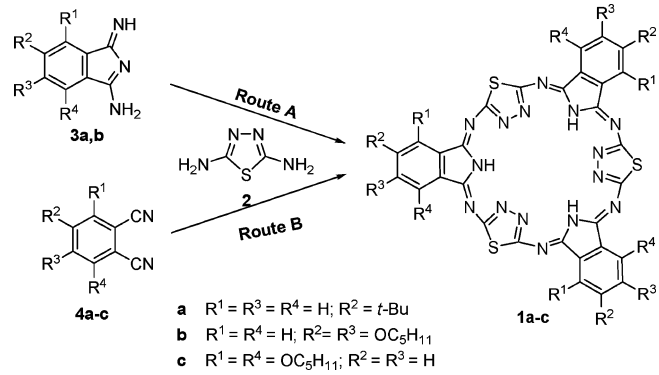

Our experience in phthalocyanine analogues[16,17] led us to report the first example of an expanded heteroazaporphyrinoid, by means of a stepwise sequence.[18] Later, we and others communicated the preparation of an expanded hemiporphyrazine **1** (Scheme 1) made up of three isoindole or pyrrole subunits, and three 1,3,4-thiadiazole moieties.[19] On the basis of its spectroscopic features and AM1 optimization of the macrocyclic geometry, we tentatively assigned a non-aromatic character to **1**, owing to a presumed deviation in the planarity of the macrocyclic core. Since then, we have been very keen to unequivocally characterize these evasive and singular compounds, and consequently, we describe here new and exciting findings on the chemistry and molecular structure of these expanded hemiporphyrazines, in addition to their complete spectroscopic, redox, and photophysical characterization.

The hexameric macrocycles **1a**−**c** were prepared in 12−59% yield by treating the corresponding phthalonitrile derivative **4a**−**c** with the thiadiazole **2** in *n*-butanol or pentanol in the presence of the corresponding sodium alkoxide (Scheme 1, route B). The efficiency of the macrocyclization reaction in terms of yield is comparable to that reported before (Scheme 1, route A)[19a] consisting in the cross-condensation of the corresponding iminoisoindolenine **3a**,**b** with 2,5-diaminothiadiazole **2**. Therefore, the overall yield of route B is considerably higher since it is one step shorter.

Compound **1a** was obtained as a mixture of the two C_1 and C_3 regioisomers (Figure 1), which were separated by standard flash chromatography. The identification of each isomer was carried out by ^{1}H NMR. Thus, while the C_3 isomer displayed a single resonance for all of the three equivalent *tert*-butyl groups

(5) Woodward, R. B. Aromaticity: An International Symposium, Sheffield, U.K., 6−9 July, 1966; *Special publication no. 21*; The Royal Chemical Society: London, U.K., 1966;
(6) (a) Sessler, J. L.; Tomat, E. *Acc. Chem. Res.* **2007**, *40*, 371–379. (b) Young, S. W.; Qing, F.; Harriman, A.; Sessler, J. L.; Dow, W. C.; Mody, T. D.; Hemmi, G. W.; Hao, Y. P.; Miller, R. A. *Proc. Natl. Acad. Sci. U.S.A.* **1996**, *93*, 6610–6615.
(7) (a) Sessler, J. L.; Gorden, A. E. V.; Seidel, D.; Hannah, S.; Lynch, V.; Gordon, P. L.; Donohoe, R. J.; Tait, C. D.; Keogh, D. W. *Inorg. Chim. Acta* **2002**, *341*, 54–70. (b) Sessler, J. L.; Vivian, A. E.; Seidel, D.; Burell, A. K.; Hoehner, M.; Mody, T. D.; Gebauer, A.; Weghorn, S. J.; Lynch, V. *Coord. Chem. Rev.* **2001**, *216*−*217*, 411–434. (c) Liao, M.-S.; Kar, T.; Scheiner, S. *J. Phys. Chem A* **2004**, *108*, 3056–3063. (d) Sessler, J. L.; Melfi, P. J.; Pantos, G. D. *Coord. Chem. Rev.* **2006**, *250*, 816–843. (e) Lynch, V. M.; Veauthier, J. M.; Gaunt, A. J.; Neu, M. P.; Ou, Z.; Kadish, K. M.; Fukuzumi, S.; Ohkubo, K.; Sessler, J. L. *Inorg. Chem.* **2007**, *46*, 5143–5145.
(8) (a) Sessler, J. L.; Davis, J. M. *Acc. Chem. Res.* **2001**, *34*, 989–997. (b) Sessler, J. L.; Camiolo, S.; Gale, P. A. *Coord. Chem. Rev.* **2003**, *240* (1−2), 17–55. (c) Kumar, M. R.; Chandrashekar, T. K. *J. Incl. Phenom. Macrocycl. Chem.* **1999**, *35*, 553–582. (d) Sessler, J. L.; Gale, P. A.; Cho, W. S. *Anion Receptor Chemistry*; Royal Society of Chemistry: Cambridge, U.K., 2006.
(9) For some examples see: (a) Xu, L.; Ferrence, G. M.; Lash, T. D. *Org. Lett.* **2006**, *8*, 5113–5116. (b) Krivokapic, A.; Cowley, A. R.; Anderson, H. L. *J. Org. Chem.* **2003**, *68*, 1089–1096. (c) Köhler, T.; Seidel, D.; Lynch, V.; Arp, F. O.; Ou, Z.; Kadish, K. M.; Sessler, J. L. *J. Am. Chem. Soc.* **2003**, *125*, 6872–6873. (d) Vogel, E.; Jux, N.; Dorr, J.; Pelster, T.; Berg, T.; Bohm, H.-S.; Behrens, F.; Lex, J.; Bremm, D.; Hohlneicher, G. *Angew. Chem., Int. Ed.* **2000**, *39*, 1101–1105. (e) Anand, V. G.; Saito, S.; Shimizu, S.; Osuka, A. *Angew. Chem., Int. Ed.* **2005**, *44*, 7244–7248. (f) Sessler, J. L.; Rubin, B. L.; Stpie, M.; Köhler, T.; Pantos, G. D.; Roznyatovskiy, V. *Can. J. Chem.* **2006**, *84*, 1218–1225.
(10) Wei, W.-H.; Fountain, M. E.; Sessler, J. L.; Magda, D. J.; Wang, Z.; Miller, R. A. *Macrocyclic Chemistry*; Gloe, K., Ed.; Springer: New York; 2005; pp 407−425.
(11) Rath, H.; Sankar, J.; PrabhuRaja, V.; Chandrashekar, T. K.; Nag, A.; Goswami, D. *J. Am. Chem. Soc.* **2005**, *127*, 11608–11609.
(12) (a) Nalwa, H. S.; Shirk, J. S. In *Phthalocyanines, Properties and Applications*; Leznoff, C. C., Lever, A. B. P., Eds.; VCH: Cambridge, 1996; Vol. 4, p 79. (b) Perry, J. W. *Nonlinear Optics of Organic Molecules and Polymers*; Nalwa, H. S., Miyata, S., Eds.; CRC Press: Boca Ratón, FL, 1997; p 813.
(13) Inokuma, Y.; Osuka, A. *Dalton Trans.* **2008**, 2517–2526.
(14) (a) Kadish, K. M., Smith, K. M., Guilard, R., Eds. *The Porphyrin Handbook*; Academic Press: San Diego, 2003; Vols. 15−20. (b) de la Torre, G.; Claessens, C. G.; Torres, T. *Chem. Commun.* **2007**, 2000–2015.
(15) (a) Sessler, J. L.; Mody, T. D.; Lynch, V. *Inorg. Chem.* **1992**, *31*, 529. (b) Marks, T. J.; Stojakovic, D. R. *J. Am. Chem. Soc.* **1978**, *100*, 1695.
(16) (a) Fernández-Lázaro, F.; Torres, T.; Hauschel, B.; Hanack, M. *Chem. Rev.* **1998**, *98*, 563–575. (b) Rodríguez-Morgade, M. S.; de la Torre, G.; Torres, T. Design and Synthesis of Low-Symmetry Phthalocyanines and Related Systems. In *Phthalocyanines: Synthesis*; Kadish, K. M., Smith, K. M., Guilard, R., Eds.; The Porphyrin Handbook, Vol. 15; Academic Press: San Diego, CA, 2003; Chapter 99, pp 125−159. (c) Rodríguez-Morgade, M. S.; Stuzhin, P. A. *J. Porphyrins Phthalocyanines* **2004**, *8*, 1129–1165. (d) Hahn, U.; Rodríguez-Morgade, M. S. *J. Porphyrins Phthalocyanines* **2009**, *13*, 455–460.
(17) (a) Nicolau, M.; Cabezón, B.; Torres, T. *Coord. Chem. Rev.* **1999**, *190*−*192*, 231. (b) Islyaikin, M. K.; Rodríguez-Morgade, M. S.; Torres, T. *Eur. J. Org. Chem.* **2002**, 2460–2464.
(18) Rodríguez-Morgade, M. S.; Cabezón, B.; Esperanza, S.; Torres, T. *Chem.—Eur. J.* **2001**, *7*, 2407–2413.
(19) (a) Islyaikin, M. K.; Danilova, E. A.; Yagodarova, L. D.; Rodríguez-Morgade, M. S.; Torres, T. *Org. Lett.* **2001**, *3*, 2153–2156. (b) Kobayashi, N.; Inagaki, S.; Nemykin, V. N.; Nonomura, T. *Angew.Chem. Int. Ed.* **2001**, *40*, 2710–2712.

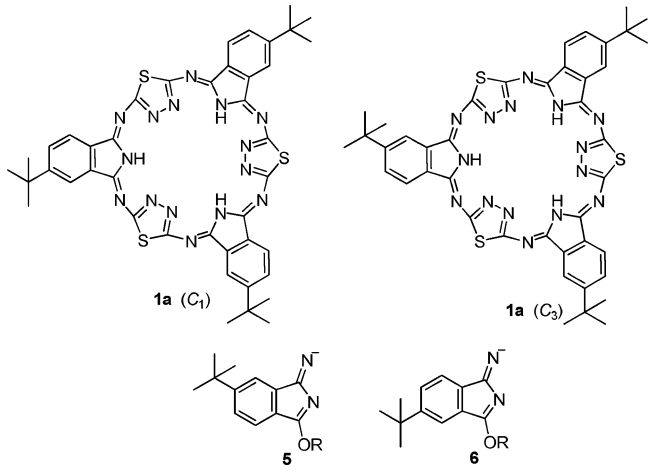

Figure 1. Structures of C_1 and C_3 regioisomers and intermediates **5**−**6**.

at $\delta = 1.45$ ppm (Figure S1 (Supporting Information)), the spectrum of the C_1 isomer (Figure S6 (Supporting Information (SI))) showed two different peaks at $\delta = 1.45$ and 1.25 ppm, integrating for 9 and 18 protons, respectively. No substantial difference was observed in the electronic spectra of these regioisomers (Figures S5 and S9 (SI)). By following both A and B pathways, only marginal yields (2−3% of the regioisomeric mixture) of isomer C_1 was isolated. This result, which greatly differs from the 75% ratio of the C_1 isomer predicted by the statistical distribution, can be attributed to the different reactivity of the two nitrile functions in **4a**. Hence, owing to the presence of the σ-donor *tert*-butyl group, the nitrile located at the first position should be more activated to nuclephilic attack than that placed at the second position. This selectively favors the formation of intermediate **5** (Figure 1), while intermediate **6** (Figure 1) is scarcely produced.[20] The generation of only one out of the two possible intermediates should be responsible for the almost exclusive formation of the C_3 isomer. In a similar manner, the preferred formation of the isoindolenine regioisomer **3a** (Scheme 1) should account for the selectivity of route A.

According to their outward aspect, compounds **1a**−**c** can be classified as expanded hemiporphyrazines,[21] and this assumption prompts the question about how effective the electronic delocalization is within the [30]heteroannulene core. In fact, one of the most remarkable features found on going from porphyrazines to hemiporphyrazines is that the latter have non-aromatic, shift-base character.[16] However, this has always been ascribed to changes in the main heteroannulene electronic circuit compared to that of porphyrazines, resulting in $4n\pi$ electron and/or cross-conjugated macrocycles. Compounds **1a**−**c** possess 30π-electrons in their most favorable π-conjugation pathway, so they should be classified as aromatic, according to Hückel's $[4n + 2]$ rule. Yet their actual nature has been puzzling so far, since their molecular structure and spectroscopic data led to an apparent contradiction. Thus, their ^{1}H NMR spectra in $CDCl_3$ showed the pyrrolic NH protons at $\delta = 11.5-12.5$ ppm, indicating very little or no diatropic ring current for these compounds. In order to discharge a dynamic equilibrium between species of different natures (i.e., Hückel aromatic and Möbius antiaromatic conformations), ^{1}H NMR spectra of **1b** at various temperatures were carried out.[4a,b,22] When the temperature increased from 25 to 115 °C, the ^{1}H NMR spectra remained unchanged; consequently, we ruled out the presence of antiaromatic species. In contrast, as the temperature decreased, compound **1b** underwent a broadening of all the signals including NH, aromatic, and aliphatic resonances, which progressively continued until splitting of the NH and aromatic peaks into three different resonances, respectively, at temperatures below −35 °C (see Figure S20 (SI)). The extent of the chemical shift variation for the inner NH protons did not go further than 1.5 ppm, so the presence of aromatic species was also discharged. A conformational desymmetrization of **1b** rather than NH tautomerism should account for the observed splitting upon decreasing the temperature, as all the signals, and not only those corresponding to NH protons, underwent splitting. Therefore, we concluded that no interconversion between Hückel and Möbius conformers was taking place within the +115 to −80 °C temperature range. The chemical shifts observed for the NH pyrrolic protons of compounds **1** in ^{1}H NMR represented a first sign of their lack of aromatic character, which we presumed arose from a distortion in the macrocyclic planarity.[19a]

Another feasible rationalization for the low-field NH signals displayed by **1** might be the presence of an aromatic macrocycle exhibiting very strong, three-centered hydrogen bonds between the inner NH protons and the two neighboring nitrogen atoms of the two side thiadiazole rings. These kind of bonding has shown to shift the involved NH protons to lower fields, so that they overcome the shielding effect of a diatropic ring current.[23] In order to discern between these two possibilities, the molecular structure of **1c** was determined using XR diffraction techniques.

Appropriate single crystals for X-ray analysis were obtained by slowly cooling a saturated solution of **1c** in acetonitrile or in chlorobenzene. The crystal structure of the expanded hemiporphyrazine **1c** confirms the inversion of the three thiadiazole rings, with the sulfur atoms pointing outward from the inner cavity.[19,24] However, the C_{3h} macrocycle exhibits a planar conformation which is obvious from the side view (Figure 2b), with a mean plane deviation of 0.051 Å (max: +0.10 and min: −0.010 Å for N_{15} and C_{14} respectively). Surprising to us the distances (2.729−2.793 Å) between the inner thiadiazole and isoindole nitrogens ($N_2\cdots N_4$) are within the hydrogen-bond range but considerably larger than that expected for a strong, three-centered hydrogen bond (∼2.5 Å).[23] So the existing hydrogen bonds can force planar conformations for **1a**−**c**, but they are too weak to shift the pyrrolic NH resonances to such a low field.[23c] A close inspection of the structure reveals some other details about the electronic delocalization in this macrocycle. Hence, the C_3-N_3 bond type is significantly shorter (1.284−1.295 Å) than the C_2-N_3 bond type (1.364−1.382 Å); that is, the former are double, whereas the latter are single bonds.

(20) Similar effects have been observed in the regioisomeric distribution of non identically substituted phthalocyanines. See: (a) Rodríguez-Morgade, S.; Hanack, M. *Chem.−Eur. J.* **1997**, *3*, 1042–1051. (b) Gaspard, S.; Maillard, P. *Tetrahedron* **1987**, *43*, 1083–1090.

(21) As in Campbell definition, half of the pyrrole rings (three) of a hypothetical porphyrazine hexamer have been replaced by another heterocycle. See: Campbell, J. B. U.S. Patent 2,765,308, 1956; *Chem. Abstr.* **1956**, *51*, 8143f.

(22) Sankar, J.; et al. *J. Am. Chem. Soc.* **2008**, *130*, 13568–13579.

(23) (a) Xue, Z.-L.; Shen, Z.; Mack, J.; Kuzuhara, D.; Yamada, H.; Okujima, T.; Ono, N.; You, X.-Z.; Kobayashi, N. *J. Am. Chem. Soc.* **2008**, *130*, 16478–16479. (b) Furuta, H.; Ishizuka, T.; Osuka, A.; Ogawa, T. *J. Am. Chem. Soc.* **1999**, *121*, 2945–2946. (c) Furuta, H.; Ishizuka, T.; Osuka, A.; Ogawa, T. *J. Am. Chem. Soc.* **2000**, *122*, 5748–5757.

(24) This has also been confirmed by gas electron diffraction: Zakharov, A. V.; Shlykov, S. A.; Danilova, E. A.; Krasnov, A. V.; Islyaikin, M. K.; Girichev, G. V. *Phys. Chem. Chem. Phys.* **2009**, *11*, 8570–8579.

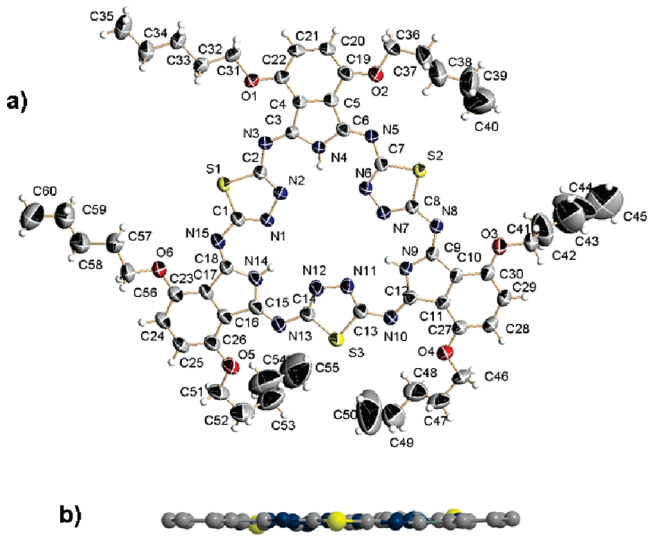

Figure 2. X-ray structure of **1c**: (a) top view; (b) side view; the peripheral substituents have been omitted for clarity.

This indicates that there is little, if any, delocalization throughout the 30-π electron heteroannulene circuit. Also remarkable is that the inner NH proton is located at the isoindole nitrogen, suggesting the presence of a single tautomer, as reflected by the observed C_3-N_4 bond type (1.371−1.386 Å) compared to the shorter (double) C_1-N_1 bond type (1.285−1.321 Å). In other words, hemiporphyrazine **1c** is planar in the solid state, this geometry being imposed by weak intramolecular hydrogen bonding. Despite its favorable conformation for the arrangement of an aromatic [30]heteroannulene, the electrons remain localized within the corresponding thiadiazole and isoindoline circuits, respectively, so that each heterocyclic subunit preserves its own aromaticity, against the overall delocalization. Therefore, aromaticity and antiaromaticity are more important concepts in small rings than in large ones,[25] a concept that has been recently illustrated by Osuka, Kobayashi, Kim and co-workers, with their report on coexistent aromatic and antiaromatic conformations of the same macrocycle.[22]

Further proof for the correct assessment of the electronic and structural properties of the above-mentioned compounds comes from calculated nucleus-independent chemical shift (NICS) values, that are becoming the most widely used tool to prove and quantify the aromatic or antiaromatic nature of a large number of molecules,[26] including expanded porphyrins.[4d] DFT calculations at the B3LYP/6-311G(d,p) level[27] as implemented in the Gaussian 03 package, revision C.02,[28] were carried out on the optimized structures. Initial geometry of **1c** was obtained from the X-ray structure, but the aliphatic chains were truncated. NICS values were obtained at the global center of the macrocycle, as well as at the center of each pyrrole, benzene, and thiadiazole rings, as shown in Figure S22 (SI). The calculated NICS(0) value for **1c** is +0.853 ppm, which clearly assigns to macrocycles **1a**−**c** a non-aromatic character.

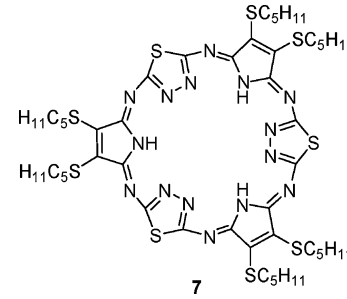

Figure 3. Expanded hemiporphyrazine **7**.

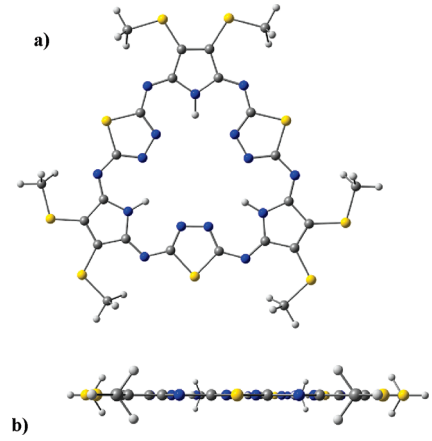

Figure 4. Optimized geometry (Cartesian coordinates) for a model of **7** with C_{3h} symmetry (a) top view; (b) side view calculated at the B3LYP/6-311G(d,p) level.

In an attempt to obtain aromatic compounds we synthesized macrocycle **7** (Figure 3) lacking fused benzene rings. By suppressing the strongly aromatic benzo groups we expected to reduce the electronic delocalization within the six heterocyclic subunits and favor the 30 π-electronic circuit. Thus, compound **7** was prepared in 3% yield by treating maleonitrile bisthiopenthoxy (**8**) with 2,5-diamino-1,3,4-thiadiazole (**2**) in butanol, in the presence of sodium butoxide and hydroquinone.[29]

The expanded hemiporphyrazine **7** was characterized by spectroscopic techniques including MS (MALDI-TOF), HRMS, UV/vis, IR, and ^{1}H and ^{13}C NMR. Thus, the MS spectra displayed the corresponding molecular ion at m/z = 1143, together with reduction peaks very typical in porphyrazine chemistry. Moreover, the UV/vis spectrum of compound **7** (Figure 5) unequivocally ascribed this macrocycle to the [3 + 3] expanded hemiporphyrazine series. The ^{1}H NMR spectrum of **7** showed the NH pyrrole signal at δ = 12.07 ppm, as diagnostic of its non-aromatic character.

X-ray analysis of compound **7** could not be obtained. Therefore, DFT calculations at the B3LYP/6-311G(d,p) level were carried out on the structure of **7**, the geometry of which was optimized by truncating the alkyl chains. We have analyzed the vibrational frequencies for warranting that the optimized structure corresponds to a minimum of energy. The main ring, with the sulfur atoms pointing out from the central cavity, is planar defining a C_{3h} symmetry. This molecular model is

(25) Fernández-Lázaro, F.; de Mendoza, J.; Mó, O.; Rodríguez-Morgade, S.; Torres, T.; Yáñez, M.; Elguero, J. *J. Chem. Soc., Perkin Trans. II* **1989**, 797–803.
(26) Chen, Z.; Wannere, C. S.; Corminboeuf, C.; Puchta, R.; von Ragué Schleyer, P. *Chem. Rev.* **2005**, *105*, 3842–3888.
(27) (a) Becke, A. D. *J. Chem. Phys.* **1993**, *98*, 5648. (b) Lee, C.; Yang, W.; Parr, R. G. *Phys. Rev. B* **1988**, *37*, 785. (c) Hehre, W. J.; Ditchfield, R.; Pople, J. A. *J. Chem. Phys.* **1972**, *56*, 2257.
(28) Frisch, M. J.; et al. *Gaussian 03*, revision C.02; Gaussian, Inc.: Wallingford CT, 2004.

(29) Two canonical forms can be outlined for compound **7**; both of them imply the coexistence of three aromatic (either pyrrole or thiadiazole) and three nonaromatic heterocyclic components within the macrocycle. We have represented compound **7** in Figure 3 according to the structure found for the benzo fused congeners **1a**−**c**.

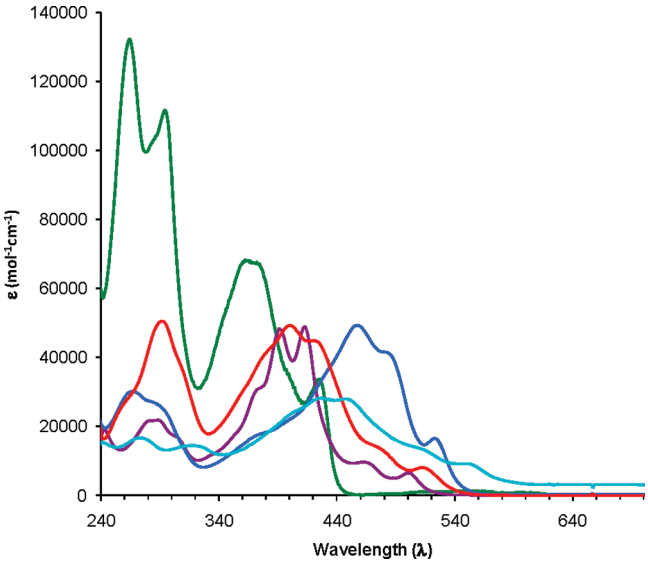

Figure 5. Optical spectra of a typical triazolohemiporphyrazine (green), **1a** (violet), **1b** (red), **1c** (blue), and **7** (cyan) in chloroform.

completely referable to the X-ray structure obtained for macrocycle **1c** (Figure 4). Moreover, the NICS value for the calculated model (−0.650 ppm) agrees with a non-aromatic structure, as in the case of **1c**.

To gain further insight into the ground state features of **1a**−**c**, we turned to absorption spectroscopy in dichloromethane. At first glance, that is, comparing the relative intensities of the spectra in the UV (250−350 nm) and visible (350−550 nm) regions, **1a**−**c** reveal striking differences. While the absorption spectrum of **1b** is marked by similar intensities, the transitions of **1a** and **1c** in the visible are more intense than those in the UV. A closer look discloses even more subtle changes in the absolute peak positions. In particular, the photophysically important long wavelength absorptions, the 0−*0 energy gaps, change, for example, from 500 nm (**1a**) to 510 nm (**1b**) and to 520 nm (**1c**)—see Figure 5. All of the remaining transitions are also impacted in the same order—**1a**: 303, 360, 392, 398, 460 nm; **1b**: 290, 380, 400, 420, 492 nm; **1c**: 283, 369, 435, 453, 480 nm (see Figure 5). The effect of the alkoxy substitution on the electronic properties of compounds **1a**−**c** follows a tendency similar to that observed in phthalocyanines upon similar peripheral functionalization. In the latter case, molecular orbital calculations have shown that meta substitution by electron-donating groups raises the energy of all frontier orbitals, this effect being slightly more pronounced for the HOMO than for the LUMO. In addition, ortho substitution produces even larger destabilization of the HOMO and only slight destabilization of the LUMO. Since the Q-band of Pcs is nearly described as a single transition from the HOMO to the LUMO frontier orbitals, these calculations match very well with experimental observations.[30]

The electrochemical properties of the macrocycles **1a**−**c** were studied using both cyclic voltammetry (Figures 6 and S23 (SI)) and differential pulse voltammetry (Figure S28 (SI)) in *o*-dichlorobenzene, being the potential window within −2.5 and +1.8 V. Tables 1 and S1 (SI) list the measured potentials determined by differential pulse voltammetry (DPV) and cyclic voltammetry (CV), respectively. The discussion will be referred to the values obtained in DPV experiments (Table 1).

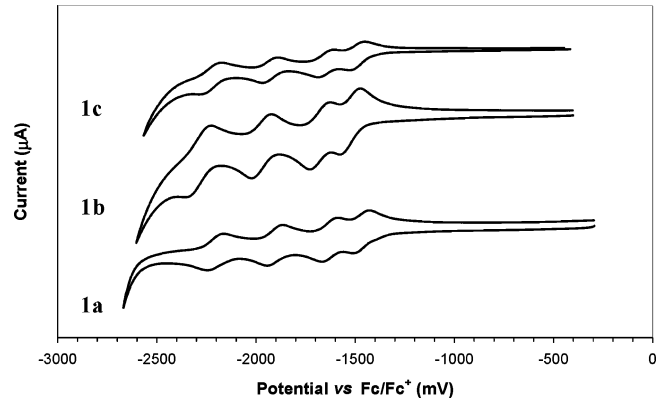

Figure 6. Cyclic voltammograms recorded on a Pt electrode (1 mm) in *o*-dichlorobenzene containing 0.1 mol L^{-1} $(n\text{-Bu})_4NPF_6$ as supporting electrolyte and **1a** (1.76×10^{-4} mol L^{-1}); **1b** (2.17×10^{-4} mol L^{-1}); **1c** (1.00×10^{-4} mol L^{-1}). Sweep rate was 100 mV s^{-1}.

Table 1. Electrochemical Reduction and Oxidation Potentials, E_p vs Fc/Fc^+ of **1a**−**c**

	potential/V, E_p vs Fc/Fc^+				
	reduction				oxidation
	$E^{0/-}$	$E^{-/2-}$	$E^{2-/3-}$	$E^{3-/4-}$	$E^{0/+}$
1a	−1.45	−1.61	−1.89	−2.19	−
1b	−1.53	−1.69	−1.97	−2.29	−
1c	−1.47	−1.63	−1.93	−2.23	+1.15

The expanded hemiporphyrazines **1a**−**c** showed four reduction peaks between −1.46 (**1a**) and −2.29 V (**1b**) (Table 1), and the three structures **1a**−**c** were considerably more difficult to get reduced (by 550−660 mV on the first reduction potential) than the similarly substituted phthalocyanines. Besides, the influence of the peripheral substitution on the potentials of the recorded redox processes followed the same tendency as for the related free-base phthalocyanines.[31] Remarkably, only compound **1c** displayed an oxidation peak within the working potential window at +1.15 V, that is 680 mV anodically shifted with respect to the corresponding *Pc*.[31] In other words, compounds **1a**−**c** are also more difficult to oxidize than the corresponding Pcs.

As a complement to the electrochemistry, the oxidized and reduced states of **1a**−**c** were tested via pulse radiolysis. Oxidation experiments were performed in oxygenated dichloromethane solution to generate $^{\bullet}OOCH_2Cl$ and $^{\bullet}OOCHCl_2$ radicals. Upon radical-induced oxidation of, for example, **1a** the kinetic traces showed that an accelerated decay of the $^{\bullet}OOCH_2Cl$ and $^{\bullet}OOCHCl_2$ radicals transforms them into a residual absorption. For **1a** a minimum at 410 nm and two sharp maxima at 440 and 500 nm are assigned to the radical cation of **1a** - see Figure 7. The spectral features that are associated with the oxidation of **1b** or **1c** are in agreement with the bathochromically shifted absorption spectra. Minima are, for example, registered at 425 nm (**1b**) and 460 nm (**1c**), while the maxima are positioned at 470/540 (**1b**) nm and 500/580 (**1c**) nm. On the time scale of the pulse radiolytic experiments, 400 μs, the one-electron oxidized forms of **1a**−**c** are stable.

The stability of the one-electron oxidized forms of **1a**−**c** was confirmed by means of spectroelectrochemistry. In particular, application of +1.5 V versus silver wire led to the same

(30) Rio, Y.; Rodríguez-Morgade, M. S.; Torres, T. *Org. Biomol. Chem.* **2008**, *6*, 1877–1894.

(31) Li, R.; Zhang, X.; Zhu, P.; Ng, D. K. P.; Kobayashi, N.; Jiang, J. *Inorg. Chem.* **2006**, *45*, 2327–2334.

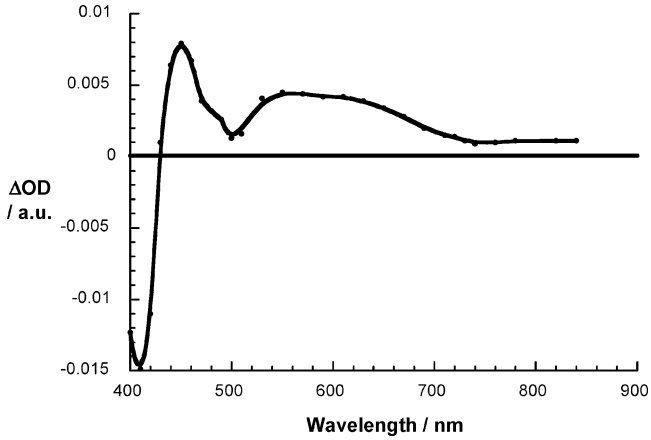

Figure 7. Differential absorption spectrum following pulse radiolytic oxidation of **1a** in oxygenated dichloromethane with $^{\bullet}OOCH_2Cl$ or $^{\bullet}OOCHCl_2$ radicals.

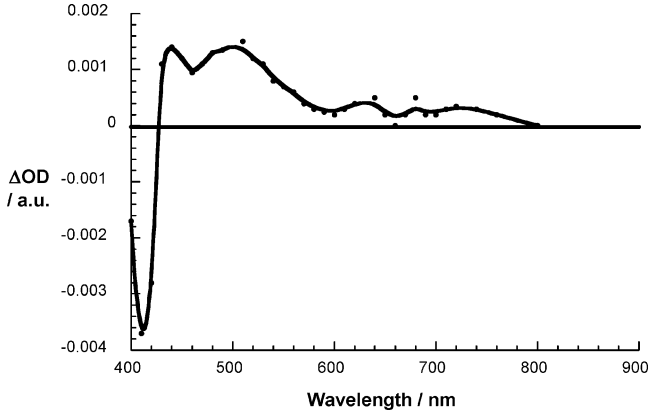

Figure 8. Differential absorption spectrum following pulse radiolytic reduction of **1a** in a deoxygenated solvent mixture containing toluene, 2-propanol, and acetone with $(CH_3)_2{}^{\bullet}COH$ and $(CH_3)_2{}^{\bullet}CO^-$ radicals.

differential absorption changes (see Figure S29 (SI)) seen upon pulse radiolytic oxidation. Moreover, a quantitative recovery of the ground state upon reverting the oxidation potential points to the complete reversibility of the oxidative process.

Achieving reductive conditions required, however, the use of a solvent mixture containing toluene, 2-propanol, and acetone rather than just pure dichloromethane. In the absence of molecular oxygen, strongly reducing $(CH_3)_2{}^{\bullet}COH$ and $(CH_3)_2{}^{\bullet}CO^-$ radicals are formed that are sufficiently reactive to reduce aromatic electron acceptors. As under oxidative conditions, a minimum is registered for **1a** at 410 nm that is accompanied by maxima at 450 and 580 nm, see Figure 8. These radical anion features are formed under pseudo-first-order conditions and are stable up to 400 μs. Again, changes in the ground state absorption spectrum, as they prevail between **1a**, **1b**, and **1c**, are also reflected in the spectrum of the one-electron reduced forms of **1a**−**c**. Radical anion features for **1c** emerge at 460, 560, and 660 nm, while those associated with the one-electron reduced form of **1b** are found at 425, 470, and 590 nm.

In contrast to the oxidation experiments, the one-electron reduced forms of **1a**−**c** turned out to be only semistable. Upon spectroelectrochemical reduction −1.5 V versus silver wire differential absorption changes (see Figure S30 (SI)) evolve that, on one hand, resemble those seen upon pulse radiolytic

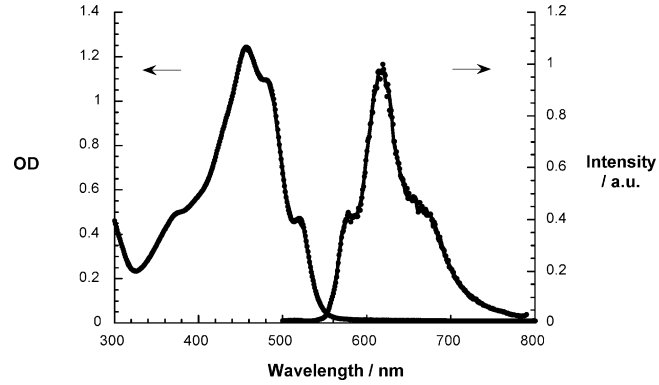

Figure 9. Room-temperature absorption spectrum and low-temperature (77 K) fluorescence spectrum of **1c** in toluene.

reduction, but, on the other hand, decay quickly due to a probable disproportionation.

Emission spectroscopy provided first insight into the excited state features of **1a**−**c**. At room temperature, visible light excitation in the range between 400 and 500 nm generates fairly broad fluorescence spectra that maximize around 600 nm (Figure 9). Nevertheless, weak shoulders are seen around 550 nm, which led us to explore the fluorescing features in a frozen matrix. Now, that is, at 77 K, a pattern evolves that is a virtual mirror image to the absorption spectrum. In particular, **1a**−**c** give rise to short wavelength fluorescence (i.e., *0−0 at 540, 570, and 575 nm) that parallel the long wavelength absorption (i.e., 0−*0 at 500, 510, and 520 nm). Notably is that the oscillator strengths of the *0−1 transitions, which emerge in the 600 nm range, are stronger than those of the *0−0 transition. The fluorescence quantum yields of **1a**, **1b**, and **1c** in dichloromethane are 0.009, 0.08, and 0.006, respectively.

In the final part, the excited state features of **1a**−**c** were looked at by transient absorption spectroscopy. All of the differential spectra recorded after the laser pulse (i.e., 150 fs laser pulses at 387 nm) in toluene or dichloromethane (see Figures 10 and 11) are best described as two sets of transient maxima. For **1a**, the transient features of the first group are located in the range between 450 and 850 nm and exhibit well-resolved fine structure (i.e., 450, 490, 560, 590, 710, 730, 760, 780, and 815 nm). In contrast, in the second group, which is seen in the 1100−1400 nm range, the features are broad (i.e., 1245 nm). Bleaching, on the other hand, of the visible absorption sets is below 450 nm. These spectral attributes are indicative of singlet−singlet transitions of **1a** as they are formed instantaneously ($>10^{12}$ s^{-1}). The singlet excited state decays rapidly (1.1×10^{10} s^{-1}) to the energetically lower-lying triplet excited state. Characteristics of the latter are limited in **1a** to a single transition that is centered at 540 nm. Superficially, the singlet−singlet features of **1b** and **1c** are similar to what has been described for **1a**. Still, bathochromic shifts are discernible (Figure 11). Most notable is the impact on the maxima in the 1100 to 1400 nm range, which are located for **1b** at 1270 nm and for **1c** at 1300 nm, although the maxima in the range between 450 and 850 nm unveil a matching trend. The singlet excited state decays of **1b** and **1c** are relatively to **1a** either decelerated (**1b**: 3.9×10^9 s^{-1}) or accelerated (**1c**: 4.3×10^{10} s^{-1}). Important is the singlet lifetime of 175 ± 10 ps, a value that is in accordance with the fluorescence lifetime measurements.[32] The accordingly formed triplets of **1b** and **1c** display

(32) Resolvable fluorescence decays were only noted for **1b**.

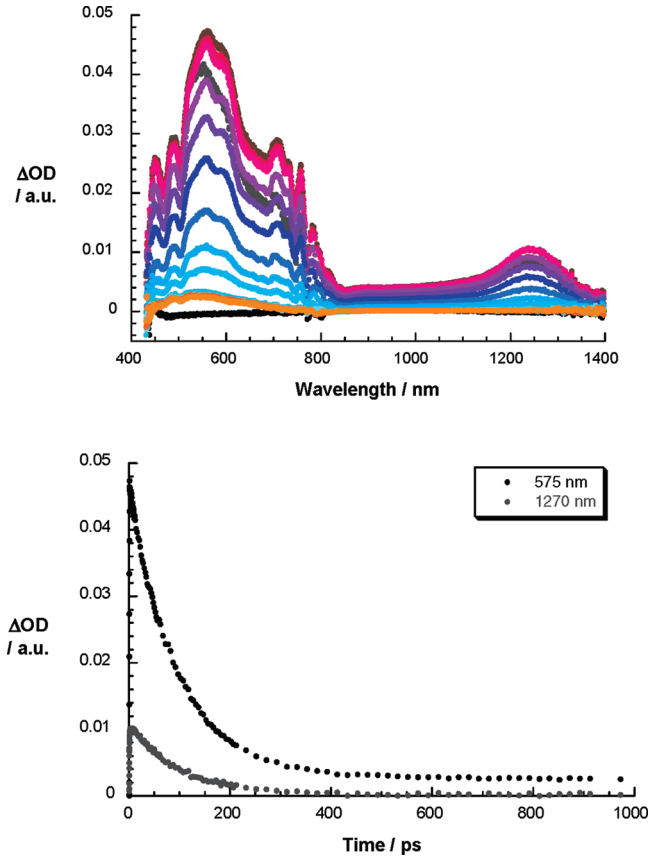

Figure 10. (Top) Differential absorption spectra (visible and near-infrared) obtained upon femtosecond flash photolysis (387 nm, −150 nJ) of **1a** in argon-saturated toluene with several time delays between 0 and 3000 ps at room temperature, illustrating the intersystem crossing. (Bottom) Time-absorption profiles at 575 and 1270 nm.

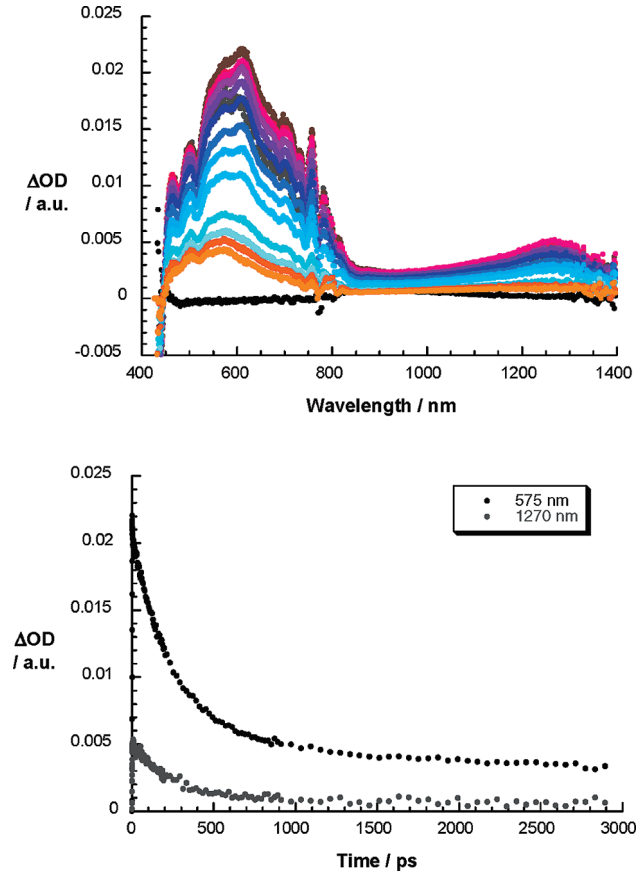

Figure 11. (Top) Differential absorption spectra (visible and near-infrared) obtained upon femtosecond flash photolysis (387 nm, −150 nJ) of **1b** in argon saturated toluene with several time delays between 0 and 3000 ps at room temperature, illustrating the intersystem crossing. (Bottom) Time-absorption profiles at 575 and 1270 nm.

in the visible (as does **1a**) red-shifted triplet−triplet maxima at 565 and 580 nm, respectively, which decay in the absence of molecular oxygen with 7.1×10^5 s^{-1} (**1a**), 1.0×10^5 s^{-1} (**1b**), and 1.0×10^5 s^{-1} (**1c**).[33] All triplet excited states turned out to be quite oxygen sensitive, with singlet oxygen quantum yields of 0.05 (**1a**), 0.60 (**1b**), and 0.11 (**1c**) in dichloromethane and were quenched with nearly diffusion-controlled kinetics to afford the formation of singlet oxygen. The quantum yields were determined via the characteristic near-infrared emission of singlet oxygen.

Conclusions

In summary, the expanded hemiporphyrazines **1a**−**c** and **7** represent rare exceptions to the Hückel [$4n + 2$] rule and evidence once more the lesser stabilization of large conjugated systems through aromaticity.[22,25] Their unique physicochemical features comprise mirror-imaged absorption and excited state fluorescence complemented by the stable formation of π-radical anions and cations by means of electrochemical and pulse radiolytical experiments. The latter are, however, short-lived, which is ascribed to the structural flexibility of the expanded hemiporphyrazines. Their large, symmetric cavity endowed with 15 nitrogen and 12 carbon atoms provide these systems with unique coordination properties, which will be reported in due course.

Experimental Section

General. Synthesis. UV/vis spectra were recorded with a Hewlett-Packard 8453 instrument. IR spectra were recorded with Bruker Vector 22 spectrophotometer. FAB-MS spectra were determined on a VG AutoSpec instrument. MALDI-TOF spectra were recorded with a Bruker Reflex III. NMR spectra were recorded with a Bruker AC-300 and Bruker DRX-500 instruments. Column chromatographies were conducted on silica gel Merck-60 (230−400 mesh, 60 Å) and aluminum oxide active neutral Merk-90 (70−230 mesh ASTM). TLC was performed on aluminum sheets precoated with silica gel 60 F_{254} (E. Merck) and aluminum oxide 60 F_{254} (E. Merck). Chemicals were purchased from Aldrich Chemical Co. and used as received without further purification. Maleonitrile **8** was prepared following reported procedures.[34]

Electrochemistry. Electrochemical measurements were performed at room temperature in a potentiostate/galvanostate Autolab PGSTAT30. Measurements were carried out in a home-built one-compartment cell with a three-electrode configuration, containing 0.1 m tetrabutylammonium hexafluorophosphate ($TBAPF_6$) as supporting electrolyte. A platinum electrode was used as the working electrode, a platinum wire as the counterelectrode and, a $Ag/AgNO_3$ nonaqueous electrode was used as reference. Prior to each voltammetric measurement the cell was degassed under an

(33) Singlet oxygen quantum yields were determined via the characteristic near-infrared emission and afforded values of 0.05 (**1**), 0.78 (**1b**), and 0.11 (**1c**).

(34) Rodríguez-Morgade, M. S.; Esperanza, S.; Torres, T.; Barberá, J. *Chem.—Eur. J.* **2005**, *11*, 354–360.

argon atmosphere for about 20 min. The solvent, ODCB, was freshly distilled from P_2O_5. The electrochemical measurements were performed by using a concentration of approximately 0.1−0.2 mmol of the corresponding compound, and ferrocene was added as an internal reference.

Photophysics. All solvents used were spectroscopic grade (99.5%) and were purchased from Sigma-Aldrich. The samples were placed in fluorimetric cuvettes with different pathways and, when necessary, purged of oxygen with argon. Femtosecond transient absorption studies were performed with 387 nm laser pulse (1 kHz, 150 fs pulse width) from an amplified Ti:Sapphire laser system (model CPA 2101, Clark-MXR Inc.). Nanosecond laser flash photolysis experiments were performed with 355 nm laser pulse from a Quanta-Ray CDR Nd:YAG system (6 ns pulse width) in a front face excitation geometry. Fluorescence lifetimes were measured by using a Fluorolog (Horiba Jobin Yvon). Steady-state fluorescence measurements were performed by using a Fluoromax 3 (Horiba Jobin Yvon). The experiments were performed at room temperature and at 77 K. Sample solutions for the frozen Matrix were prepared using methyltetrahydrofuran (MTHF) and freezing the solutions by liquid N_2 to 77 K. Pulse radiolysis experiments were performed using 50 ns pulses of 15 MeV electrons from a linear electron accelerator (LINAC). Dosimetry was based on the oxidation of SCN^- to$(SCN)_2^{\bullet-}$ which in aqueous, N_2O-saturated solution takes place with $G \approx 6$ (G denotes the number of species per 100 eV, or the approximate μm concentration per 10 J absorbed energy). The radical concentration generated per pulse was varied between $(1-3) \times 10^{-6}$ M.

General Procedure for the Preparation of Compounds 1a,b. A solution of the corresponding phthalonitrile **4a**,**b** (1.0 mmol) in dry butanol (8 mL) was stirred with sodium butoxide (0.5 mmol) under argon at room temperature for 12 h, and afterward 2,5-diamino-1,3,4-thiadiazole (**2**) (1.0 mmol) was added. The mixture was stirred under argon at room temperature for 1 h, warmed up to 100 °C, and stirred for 12 h. After refluxing for another 12 h, the mixture was allowed to cool to room temperature. The solvent was rotary evaporated, and the residue was suspended in hexanes (10 mL), filtered, and washed with methanol. The solid was dissolved in chloroform and filtered through aluminum oxide. The macrocycles were purified by column chromatography on silica gel.

1a: Eluent: chloroform. Yield: 59%. Orange solid. The C_1 isomer eluted before the C_3 isomer.

1a-C$_1$: ^{1}H NMR (300 MHz, $CDCl_3$): δ = 12.63 (bs, 3H, NH), 8.10 (s, 3H, H arom), 7.96 (d, 3H, H arom), 7.7−7.6 (m, 3H, H arom), 1.46 (s, 9H, CCH_3), 1.25 (s, 18H, CCH_3); IR (KBr): ν = 3271, 3231 (NH), 2920, 2853 (C−H), 1624, 1462, 1408, 1367, 1259, 1219, 1084, 1030, 841, 800, 760 cm^{-1}; UV/vis ($CHCl_3$): λ_{max} (log ε/dm^3 mol^{-1} cm^{-1}) = 287 (2.34), 393 (4.84), 413 (4.91), 462 (1.05), 500 (0.70) nm; MS (FAB, NBA): m/z = 850 $[M + H]^+$, 888 $[M + K]^+$, 981 $[M + Cs]^+$.

1a-C$_3$: ^{1}H NMR (300 MHz, $CDCl_3$): δ = 12.55 (bs, 3H, NH), 8.05 (s, 3H, H arom), 7.90 (d, 3H, H arom), 7.7−7.6 (m, 3H, H arom), 1.45 (s, 27H, CCH_3); ^{13}C NMR (75.5 MHz, $CDCl_3$): δ = 169.8, 156.8, 153.4, 153.2, 134.7, 132.0, 129.9, 122.9, 120.1, 35.7 ($C(CH_3)_3$), 31.3 ppm ($C(CH_3)_3$); IR (KBr): ν = 3231 (NH), 2961, 2920, 2852 (C−H), 1624, 1489, 1408, 1367, 1219, 1030, 841, 746, 719 cm^{-1}; UV/vis ($CHCl_3$): λ_{max} (log ε/dm^3 mol^{-1} cm^{-1}) = 276 (4.31), 303 (4.37), 360 (4.47), 392 (4.67), 398 (4.69), 460 (3.98), 500 (3.90) nm; MS (FAB, NBA): m/z = 850 $[M + H]^+$, 888 $[M + K]^+$, 981 $[M + Cs]^+$.

1b: Eluent: chloroform/methanol (10:1). Yield: 29%. ^{1}H NMR ($CDCl_3$, 500 MHz, TMS): δ = 11.03 (s, 3H, NH), 6.61 (s, 6H, arom), 3.71 (m, 12H, CH_2), 1.77 (m, 12H, CH_2), 1.45 (m, 24H, CH_2), 0.98 ppm (m, 18H, CH_3); ^{13}C NMR ($CDCl_3$, 75.5 MHz,): δ = 169.1, 152.4, 126.7, 104.6, 68.8 (OCH_2), 29.1 (CH_2), 28.2 (CH_2), 22.68 (CH_2), 14.05 ppm (CH_3); IR (KBr): ν = 3273, 3232 (N−H), 2955, 2928, 2860 (C−H), 1639, 1489, 1462, 1367, 1273, 1219, 1124, 1016, 897, 793, 717, 677 cm^{-1}; UV/vis ($CHCl_3$): λ_{max} (log ε/dm^3 mol^{-1} cm^{-1}) = 290 (4.69), 380 (4.61), 400 (4.69), 420 (4.65), 492 (4.20), 510 (3.90) nm; MS (MALDI-TOF, dithranol): m/z = 1198.6 $[M + H]^+$, 1236.5 $[M + K]^+$; HRMS (MALDI-TOF) calcd for $C_{60}H_{76}N_{15}O_6S_3$ $[M + H]^+$: 1198.526, found: 1198.530; analysis calcd (%) for $C_{60}H_{76}N_{15}O_6S_3 \cdot 2H_2O$: C = 58.37, H = 6.45, N = 17.02, S = 7.79; found: C = 58.06, H = 6.33, N = 17.00, S = 7.16.

Preparation of 1c. 3,6-Dipentoxyphthalonitrile (**4c**, 300 mg, 1.0 mmol) and 2,5-diamino-1,3,4-thiadiazole (116 mg, 1.0 mmol) were refluxed in dry pentanol (8 mL) until the solution became homogeneous. Sodium (12 mg, 0.5 mmol) was added, and the reaction mixture was refluxed for 32 h under argon. Afterward, the pentanol was rotary evaporated, and the residue was suspended in hexane (10 mL), filtered, and washed with methanol followed by ether. The obtained solid was dissolved in chloroform and filtered through aluminum oxide. Purification by column chromatography on silica gel using chloroform as eluent afforded 144 mg of **1c** (12%) as a red solid. ^{1}H NMR ($CDCl_3$, 500 MHz): δ = 12.71 (s, 3H, NH), 7.13 (s, 6H, H arom), 1.48 (m, 12H, CH_2), 4.18 (m, 12H, OCH_2), 1.96 (m, 12H, CH_2), 1.63 (m, 12H, CH_2), 1.48 (m, 12H, CH_2), 0.10 ppm (m, 18H, CH_3); ^{13}C NMR ($CDCl_3$, 75.5 MHz,): δ = 170.3, 152.2, 150.9, 121.8, 119.0, 69.8 (OCH_2), 29.0 (CH_2), 28.4 (CH_2), 22.6 (CH_2), 14.2 ppm (CH_3); IR (KBr): ν = 3223 (N−H), 2935, 2868 (C−H), 1616, 1508, 1468, 1400, 1427, 1373, 1283, 1256, 1188, 1121, 1068, 966, 918, 883, 837, 800, 735, 613 cm^{-1}; UV/vis ($CHCl_3$): λ_{max} (log ε/dm^3 mol^{-1} cm^{-1}) = 266 (4.46), 283 (4.43), 369 (4.20), 435 (4.58), 453 (4.68), 480 (4.62), 520 (4.19) nm; MS (MALDI-TOF, dithranol): m/z = 1200 $[M + H]^+$; HRMS (MALDI-TOF) calcd for $C_{60}H_{76}N_{15}O_6S_3$ $[M + H]^+$: 1198.526, found: 1198.528; analysis calcd (%) for $C_{60}H_{76}N_{15}O_6S_3$: C = 60.13, H = 6.31, N = 17.53, S = 8.03; found: C = 60.26, H = 6.47, N = 17.16, S = 7.63.

Preparation of 7. A solution of the thiadiazole **2** (116 mg, 1 mmol), hydroquinone (7 mg, 0.06 mmol), and freshly prepared NaBuO (0.5 mmol) in dry butanol (3 mL) was stirred under Ar at room temperature for some minutes until the solution became yellow, and then the maleonitrile **8** (282 mg, 1 mmol) was added. The mixture was stirred at room temperature and protected from light for 23 h, and then the temperature was gradually raised up to reflux. The solution was refluxed for 18 h, and then the solvent was rotary evaporated, and the residue was sequentially washed with water and hexanes. The obtained solid was chromatographed on silica gel using $CHCl_3$ as eluent. Further gel permeation chromatography (Biobeads SX-1, THF) afforded **7** (34 mg, 3%) as a red solid. ^{1}H NMR ($CDCl_3$, 300 MHz): δ = 12.08 (s, 3H, NH), 3.38 (t, J = 6 Hz, 12H, SCH_2), 1.72 (quin, J = 6 Hz, 12H, CH_2),1.5−1.3 (m, 24H, CH_2), 0.91 ppm (t, J = 6 Hz, 18H, CH_3); ^{13}C NMR ($CDCl_3$, 75.5 MHz,): δ = 170.0 (C═N), 154.0 (C═N), 139.7 (C═C), 33.4 (SCH_2), 30.8 (CH_2), 30.0 (CH_2), 22.3 (CH_2), 14.1 ppm (CH_3); IR (KBr): ν = 3236 (N−H), 2951, 2924, 2851 (C−H), 1736, 1597, 1431, 1400, 1458, 1192, 1107, 1045 cm^{-1}; UV/vis ($CHCl_3$): λ_{max} (log ε/dm^3 mol^{-1} cm^{-1}) = 272 (4.22), 317 (4.16), 427 (4.45), 448 (4.45), 506 (4.12), 553 (3.96) nm; MS (MALDI-TOF, dithranol): m/z = 1143−1152 $[M]^+$, $[M + H]^+$, $[M + 2H]^+$, $[M + 3H]^+$; HRMS (MALDI-TOF) calcd for $C_{48}H_{69}N_{15}S_9$ $[M]^+$: 1143.335; found: 1143.344.

Experimental X-ray Diffraction of 1c·Acetonitrile and 1c·Chlorobenzene. Red parallelepiped-shaped crystals of **1c**·acetonitrile and **1c**·chlorobenzene, of dimension 0.20 mm × 0.34 mm × 0.42 mm and 0.12 mm × 0.20 mm × 0.34 mm, respectively, were selected under a polarizing optical microscope. **1c**·acetonitrile data were collected at room temperature, while **1c**·chlorobenzene data were collected at 173 K using an Oxford N-HELIX device (Oxford Cryosystem), on a Bruker four circle kappa diffractometer equipped with a Cu INCOATEC microsource operated at 30 W power (45 kV, 0.60 mA) to generate Cu Kα radiation (λ = 1.54178 Å), and a Bruker AXIOM area detector (microgap technology). Diffraction data were collected exploring over a hemisphere of the reciprocal space in a combination of ϕ and ω scans to reach a resolution of 0.82 Å (62.69° in θ) for

1c·acetonitrile and 0.87 (58.90° θ) for **1c**·chlorobenzene, using a Bruker APEX2 software suite1. Unit cell dimensions were determined by a least-squares fit of reflections with $I > 2\ \sigma(I)$. Data were integrated and scaled using SAINTplus and SCALE programs.[35] The structure was solved by direct methods using SHELXS,[35] showing all non-hydrogen atoms and additional cycles of refinement and electron difference maps showing the rest of the atoms. Final refinement was carried out by anisotropic full-matrix least-squares, except for hydrogen atoms, which were included with isotropic thermal parameters using SHELXL.[35] Both structures are quite similar and crystallize with a solvent molecule by **1c** molecule. A summary of the main crystallographic data are shown in Tables S2a and S2b (SI), atomic coordinates and equalized thermal parameters are shown in Tables S3a and S3b (SI), and bond lengths and angles are shown in Tables S4a (acetonitrile) and S4b (chlorobenzene) (SI). ORTEP representations of the asymmetric unit are shown in Figures S21a (acetonitrile) and S21b (chlorobenzene) (SI).

(35) *Apex II Suite*; Bruker AXS Inc.: Madison, Wisconsin, U.S.A, 2006.

Acknowledgment. Dedicated to Professor Karl M. Kadish on the occasion of his 65th birthday. This work has been supported by the Spanish MEC (CTQ-2008-00418/BQU and CONSOLIDER INGENIO 2010, CSD2007-00010), the Comunidad de Madrid (MADRISOLAR-2, S2009/PPQ/1533), and the Deutsche Forschungs-Gemeinschaft (SFB 583). We acknowledge Dr. Victor Ferro (UAM) for DFT calculations.

Supporting Information Available: Complete refs 22 and 28; characterization data for compounds **1a**−**c** and **7** (^{1}H NMR, ^{13}C NMR, UV/vis, IR, MS, and electrochemical redox potentials from CV experiments). This material is available free of charge via the Internet http://pubs.acs.org.

JA104577D